



OPEN

Simultaneous removal of SO₂ and NO_x from flue gas by low-temperature adsorption over activated carbon

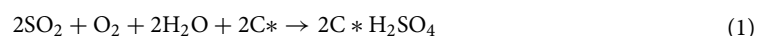
Shiqing Wang^{1✉}, Shisen Xu², Shiwang Gao³, Ping Xiao⁴, Minhua Jiang², He Zhao², Bin Huang², Lianbo Liu¹, Hongwei Niu¹, Jinyi Wang³ & Dongfang Guo³

An exceptional phenomenon has been observed that SO₂ and NO_x in flue gas can be effectively adsorbed over activated carbon with a surprising capacity at cold temperatures with the presence of oxygen. In this study, the adsorption characteristics of NO and SO₂ over activated carbon at 80, 20, 0, and –20 °C is experimentally investigated. Without the presence of oxygen, adsorption of NO is negligible. In the presence of oxygen, NO can be oxidized to NO₂ over activated carbon which leads to the co-adsorption of NO/NO₂ within the adsorption bed. Catalytic oxidation of NO over activated carbon can be significantly enhanced at cold temperatures, leading to an extraordinary increase of adsorption capacity of NO. With an initial concentration of NO = 200 ppmv and a space velocity of 5000 h⁻¹, the average specific capacity increases from 3.8 to 169.1 mg/g when the temperature decreases from 80 to –20 °C. For NO–O₂ co-adsorption, the specific capacity increases along the adsorption bed due to the increasing NO₂ concentrations. The adsorption capacity of SO₂ is also significantly enhanced at cold temperatures. With an initial concentration of SO₂ = 1000 ppmv, the specific capacity increases from 12.9 to 123.1 mg/g when the temperature decreases from 80 to –20 °C. A novel low-temperature adsorption (LAS) process is developed to simultaneously remove SO₂ and NO_x from flue gas with a target of near-zero emission. A pilot-scale testing platform with a flue gas flowrate of 3600 Nm³/h is developed and tested. Emission of both SO₂ and NO_x is less than 1 ppmv, and the predicted energy penalty is about 3% of the net generation.

SO₂ and NO_x in flue gas are major air pollutants responsible for acid rain and photochemical smog. SO₂ is an acidic gas and can be scrubbed by alkalic solutions such as lime, sodium carbonate, ammonia, etc.^{1,2}. Seawater is also considered as a scrubbing agent for desulfurization^{3,4}. NO_x is composed of various forms of nitrogen oxides such as NO, NO₂, N₂O, etc. The dominant species is nitrogen monoxide (NO) which can be either reduced to N₂ by selective catalytic reduction or oxidized to NO₂ which can be scrubbed by alkalic solutions⁵. Wet flue gas desulfurization (WFGD) and SCR dinitrification are the dominant technologies in power plants nowadays.

In addition, adsorption technology has also been widely used for gas cleanup. Simultaneous removal of SO₂ and NO_x by activated carbon or coke has been successfully demonstrated in flue gas treatment^{6,7}. A schematic drawing of the process is shown in Fig. 1.

Activated coke technology can remove SO₂, NO_x, Hg and other adsorbable pollutants simultaneously⁸. The removal of SO₂ over activated carbon in the presence of oxygen and moisture involves a series of reactions that leads to the formation of sulfuric acid. The used carbon is regenerated through heating to recover their adsorbing activity. The desorbed SO₂ is recycled as elemental sulfur, sulfuric acid or liquid SO₂, as shown in Fig. 1. And the desorbed Hg and other trace contaminant species can be separated and collected during the sulfuric acid or sulfur production process. The typical operating temperature is 80–150 °C in the adsorber and 350–450 °C in the regenerator. The overall adsorption and desorption reactions are as follows⁹:



¹Huaneng Clean Energy Research Institute, Beijing 102209, China. ²China Huaneng Group Co., Ltd., Beijing 100031, China. ³Beijing Key Laboratory of CO₂ Capture and Process, Beijing 102209, China. ⁴State Key Laboratory of Coal Based Clean Energy, Beijing 102209, China. ✉email: sq_wang@qny.chng.com.cn

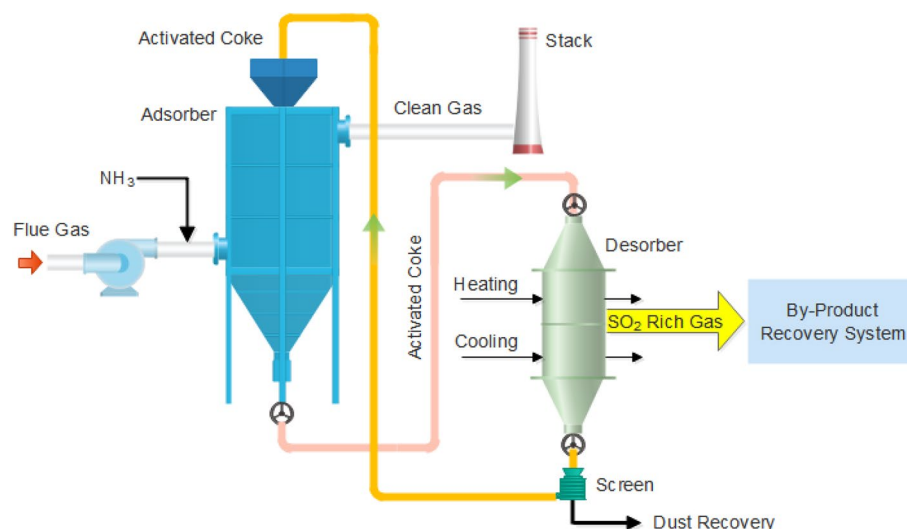


Figure 1. Schematic drawing of the activated coke desulfurization and denitrification process.



For activated coke technology, NO_x is not removed by adsorption. It is removed through catalytic reduction over activated carbon by reacting with injecting NH_3 , which converts NO_x to non-toxic gas N_2 . The overall reactions are as follows¹⁰:



Activated coke technology has been widely used for sintering flue gas treatment in iron and steel industry¹¹, but only a few applications in power plants have been reported¹². Power plant flue gas normally has a much higher concentration of SO_2 and larger flowrate than sintering flue gas, the specific capacity of SO_2 is not sufficient enough to treat the power plant flue gas. To improve the adsorption capacity, researchers have also investigated the possibility of using other adsorbents such as modified activated carbon^{13,14}, activated carbon fibers¹⁵, molecular sieve^{16,17}, alumina substrate impregnated with sodium carbonate¹⁸, copper oxide¹⁹, etc. But none of these adsorbents has been successfully commercialized.

Another defective feature of traditional activated coke technology is that NO_x is not able to be removed effectively through adsorption and the injection of ammonia is required to improve the denitrification rate. The removal rate of NO_x is less than 20% without NH_3 and can be increased to around 70% if sufficient NH_3 is injected^{7,20}.

This study proposed a novel low-temperature adsorption (LAS) technology which is able to remove both SO_2 and NO_x through adsorption with extraordinary adsorption capacity and high efficiency. The development of LAS technology is inspired by an interesting phenomenon observed accidentally that NO_x can be adsorbed by activated carbon effectively with an astonishing capacity when flue gas is cooled to cold temperatures. The fundamental behaviors of NO and SO_2 adsorption at cold temperatures over activated carbon is investigated in this study. Furthermore, a pilot-scale testing platform with a flue gas treatment capacity of $3600 \text{ Nm}^3/\text{h}$ is designed and built to validate the performance of LAS technology. A brief introduction and first-hand data from the pilot-scale testing facility is also shared in this study. But the detail results from the pilot tests will be discussed in the future.

A comparison between the LAS technology and traditional activated coke technology is given in Table 1. The specific capacity is obtained in this study. The removal rate of traditional activated coke technology is from reported literature⁷ and the removal rate of LAS technology is obtained from the pilot platform.

Method

Material. Commercial coconut activated carbon (CAC) with granular size between 26 and 30 mesh is used in this study. The surface physical properties of CAC is characterized by BET method (Quantachrome QUADRASORB SI). The specific surface area of CAC is $1314.5 \text{ m}^2/\text{g}$, the pore size is mainly smaller than 2 nm, as shown in Fig. 2, in which DFT method is used to determine the pore size distribution. CAC is pretreated by heating to $300 \text{ }^\circ\text{C}$ in a vacuum tube for 2 h before each test. Mass of CAC is measured after the pretreatment. The loading density of granular CAC is $0.5 \text{ g}/\text{cm}^3$.

Experimental setup. Figure 3 is a schematic drawing of the experimental setup for investigating the adsorption behaviors of SO_2 and NO at cold temperatures. The dry flue gas has a volume flow rate of $Q = 1 \text{ L}$

Items	Traditional activated coke technology	Low-temperature adsorption technology
Adsorption temperature	80–150 °C	– 20–5 °C
SO ₂ removal method	Adsorption	Adsorption
NO _x removal method	Catalytic reduction	Adsorption
Specific capacity of SO ₂	11.31 mg/g at 80 °C	147.61 mg/g at – 20 °C
Specific capacity of NO _x	0.27 mg/g at 80 °C	13.24 mg/g at – 20 °C
SO ₂ removal rate	90–98%	≥ 99.9%
NO _x remove rate	70–80% (with NH ₃ injection)	≥ 99%
Injection of NH ₃	Required	Not required
Flue gas cooling system	Not required	Required
Adsorber	Large	Small

Table 1. Comparison of LAS technology and traditional activated coke technology.

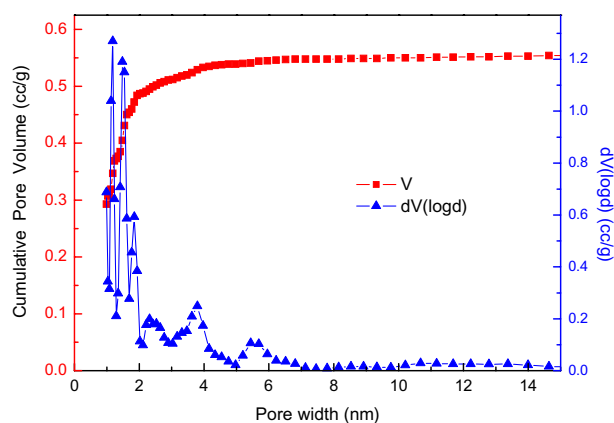


Figure 2. Pore distribution of coconut activated carbon (V: pore volume; dV: reciprocal of volume).

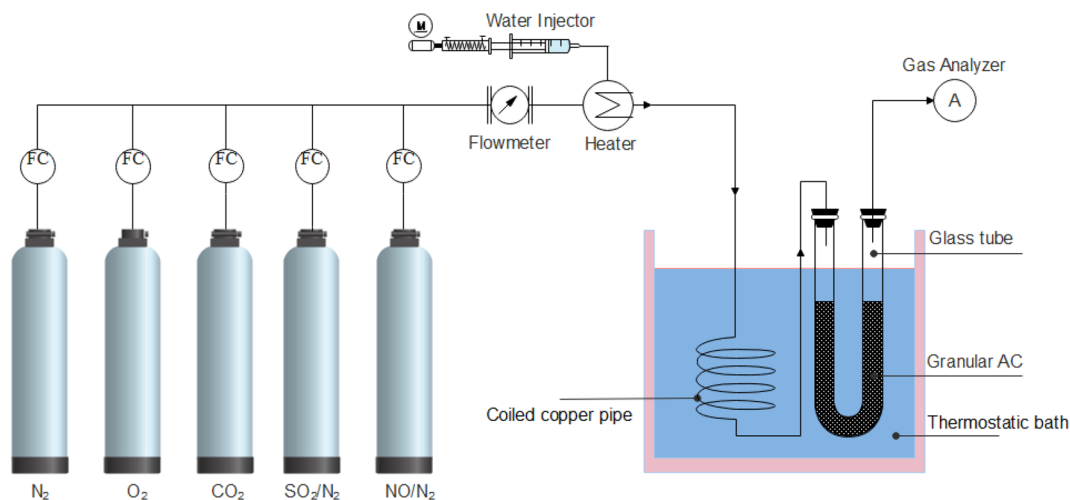


Figure 3. Experimental setup for low-temperature adsorption of SO₂ and NO.

min, and has a volume concentration of N₂ = 82%, O₂ = 6%, CO₂ = 12%, SO₂ = 1000 ppmv and NO = 200 ppmv. Moisture in flue gas is added by a water injector controlled by a stepper motor. At 80 °C, 10 vol.% of H₂O is added to the flue gas. At 20, 0 and – 20 °C, the concentration of H₂O is reduced to the saturated moisture content at corresponding temperatures, which are 2.3, 0.6 and 0.1 vol.%, respectively. This is because the extra moisture will be removed from the flue gas during cooling process. The flue gas is pre-heated or pre-cooled to adsorption temperature by a coiled copper pipe immersing in a thermostatic bath with a temperature range of – 40 to

Component	Method	Range	Accuracy	Resolution
CO ₂	IR sensor	0–25 vol.%	± 0.3 vol.%	0.01 vol.%
O ₂	Electrochemical sensor	0–25 vol.%	± 0.2 vol.%	0.01 vol.%
SO ₂	Electrochemical sensor	0 ~ +5000	± 5% of measured value	1 ppmv
NO	Electrochemical sensor	0 ~ +4000 ppmv	± 5% of measured value	1 ppmv
NO ₂	Electrochemical sensor	0 ~ +500 ppmv	± 5% of measured value	0.1 ppmv

Table 2. Basis information of gas analyzer TESTO 350.

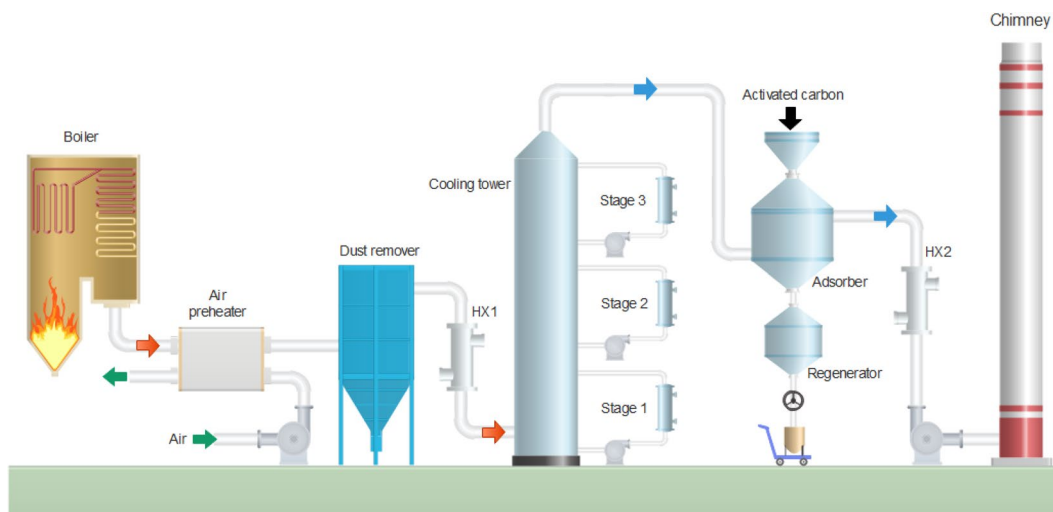


Figure 4. Schematic flowchart of pilot-scale test platform.

100 °C. The granular activated carbon is loaded in a glass tube with an inner diameter of 5 mm which is also immersed in the thermostatic bath. The difference between bath temperature and the gas temperature at the exit of adsorption bed is less than 2 °C. During each test, 6 g of CAC is loaded and the space velocity of adsorption bed is 5000 h⁻¹. The gas composition of flue gas leaving the adsorption tube is measured by flue gas analyzer testo 350. The gas analyzer is capable of measuring O₂, CO₂, SO₂, NO and NO₂. The method, accuracy and resolution of the analyzer for each component is given in Table 2.

Pilot platform. A pilot-scale test platform is designed to simultaneously remove SO₂, NO_x and other adsorbable pollutants based on the novel low-temperature adsorption technology. The designed flue gas flowrate is 3600 Nm³/h. The adsorption temperature is between - 20 to 5 °C. The pollutants control target is near-zero emission: SO₂ and NO_x ≤ 1 ppmv.

A schematic flowchart of the pilot-scale test platform is shown in Fig. 4. Flue gas is extracted from the inlet duct before SCR denitrification system. Hot flue gas is cooled to around 120 °C by an air preheater and the dust is then removed by a bag-type dust remover. Flue gas is further cooled to around 70 °C by a residue heat recovery exchanger (HX1) which can generate usable hot water. Flue gas is cooled to cold temperatures by a direct contact cooling (DCC) tower which has three cooling stages. In the lower stage (stage 1), flue gas is cooled close to room temperature by water scrubbing and the cooling load is provided by cooling water; in the second stage (stage 2), flue gas is cooled to 2–5 °C by cold water scrubbing and the cooling load is provided by an industrial chiller; in the upper stage (stage 3), flue gas is cooled to below freezing point by calcium chloride solution scrubbing and the cooling load is provided by an industrial refrigerator. The cold flue gas enters the adsorber in which SO₂ and NO_x are removed by activated carbon through adsorption. The cold energy of clean flue gas is recovered by cooling the scrubbing water in the DCC cooling tower through HX2. The saturated activated carbon is heated in the regenerator to recover its adsorption activity for repeatable utilization. The desorbed SO₂ can be recovered as elemental sulfur or sulfuric acid, and the desorbed NO_x can be introduced to the boiler to form a stable thermal balance of NO_x-N₂-O₂, which has been successfully demonstrated in the NO_x SO process¹⁸. In this pilot study however, the post-treatment of desorbed gas is not considered.

Results and discussion

Phenomenon. This section is to introduce an interesting observation on the adsorption of SO₂ and NO at cold temperatures, which to our knowledge has not yet been reported in open literature. This phenomenon is the origin of this study as well as the development of LAS technology.

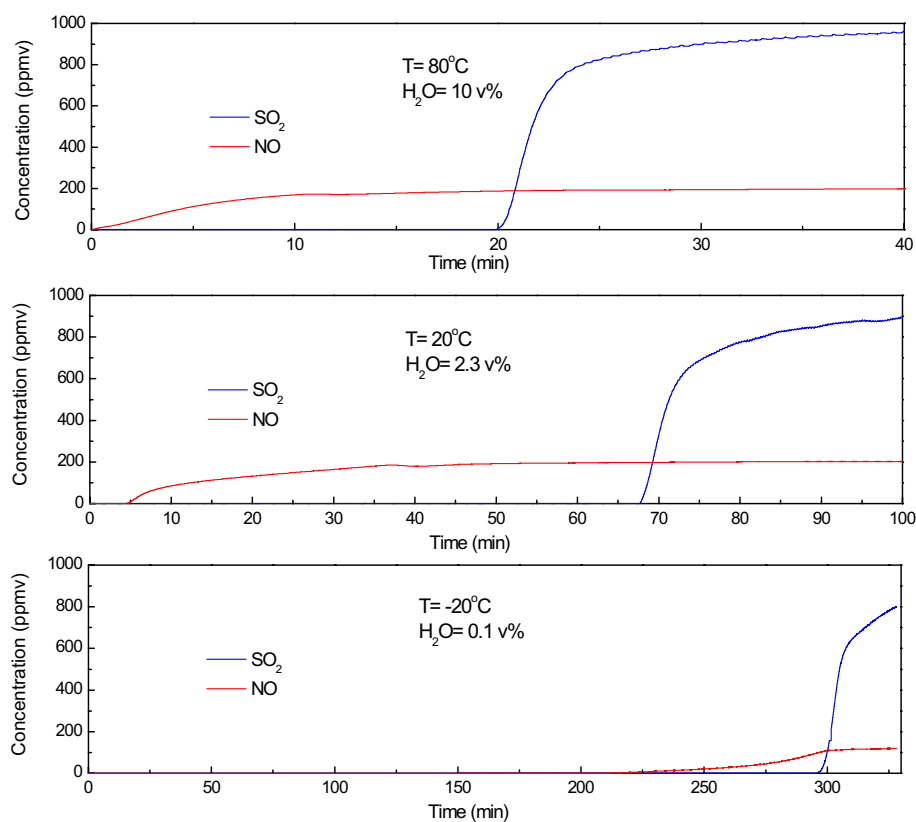


Figure 5. Breakthrough curves of SO₂ (blue) and NO (red) adsorption at 80, 20 and – 20 °C (Simulated flue gas: SO₂ = 1000 ppmv, NO = 200 ppmv, O₂ = 6 vol.%, CO₂ = 12 vol.%, space velocity = 5000 h⁻¹).

The adsorption characteristics of SO₂ and NO at 80, 20 and – 20 °C is investigated by the experimental setup shown in Fig. 3. The simulated flue gas has a composition described in section “Experimental setup”. During each test, 6 g of CAC is loaded in the tube and the space velocity is 5000 h⁻¹. The concentration of SO₂ and NO is 1000 and 200 ppmv, respectively. The dry flue gas has a volume flow rate of 1 L/min. The water content is 10 vol.% at 80 °C, 2.3 vol.% (saturated) at 20 °C, 0.1 vol.% (saturated) at – 20 °C, respectively.

Figure 5 is the breakthrough curve of SO₂ (blue) and NO (red) of the three experiments. The concentrations of SO₂ and NO leaving the adsorption bed (C_{out}) are measured and plotted. Since the gas analyzer has a resolution of 1 ppmv for both SO₂ and NO, the breakthrough time (t_b , min) is defined as the time when $C_{out}(SO_2) = 1$ ppmv and $C_{out}(NO) = 1$ ppmv. The breakthrough adsorption capacity (A_b , mg/g) is defined as the adsorption capacity which can maintain near-zero emission (less than 1 ppmv). The saturated adsorption capacity (A_s , mg/g) is defined as the maximum adsorption capacity when the bed stops adsorption. These two specific capacities are key parameters which determine the loading space velocity of adsorption bed and the frequency of bed regeneration.

The breakthrough and saturated adsorption capacity are calculated by the following equations:

$$A_b = \frac{C_{in} \times t_b \times Q \times M}{22.4 \times m} \times 10^{-3} \quad (5)$$

$$A_s = \frac{\int_{t_0}^{t_e} (C_{in} - C_{out}(t)) \times Q \times M \times dt}{22.4 \times m} \times 10^{-3} \quad (6)$$

where A_b and A_s are the breakthrough and saturated adsorption capacity (mg/g), respectively. t_b (min) is the breakthrough time. Q (L/min) is the flow rate of simulated flue gas, which is 1 L/min. M (g/mol) is the molecular weight of SO₂ or NO. m (g) is the mass of loaded CAC, which is 6 g when the space velocity is 5000 h⁻¹. C_{in} (ppmv) is the inlet concentration, which is 1000 ppmv for SO₂ and 200 ppmv for NO. $C_{out}(t)$ is the outlet concentration of SO₂ or NO at time t (min). In the time integral of Eq. (6), t_0 is the starting time and t_e is ending time when the bed stops adsorption ($C_{out} = C_{in}$).

As shown in Fig. 5, NO breaks through the adsorption bed almost instantaneously at an adsorption temperature of 80 °C which is close to the operating temperature of traditional activated coke technology. The breakthrough time of NO is about 5 min at 20 °C and 225 min at – 20 °C. The breakthrough time of SO₂ is 20, 68 and 295 min at 80, 20 and – 20 °C, respectively. The specific capacity of SO₂ and NO calculated by Eqs. (5) and (6) is given in Table 3.

Temperature (°C)	NO			SO ₂		
	<i>t_b</i> (min)	<i>A_b</i> (mg/g)	<i>A_s</i> (mg/g)	<i>t_b</i> (min)	<i>A_b</i> (mg/g)	<i>A_s</i> (mg/g)
80	0.05	0.002	0.27	20	9.52	11.31
20	5	0.22	0.80	68	32.38	37.18
-20	225	10.07	13.24	295	140.47	147.61

Table 3. Adsorption capacity of SO₂ and NO co-adsorption over CAC at various temperatures (simulated flue gas: SO₂ = 1000 ppmv, NO = 200 ppmv, O₂ = 6 vol.%, CO₂ = 12 vol.%, space velocity = 5000 h⁻¹).

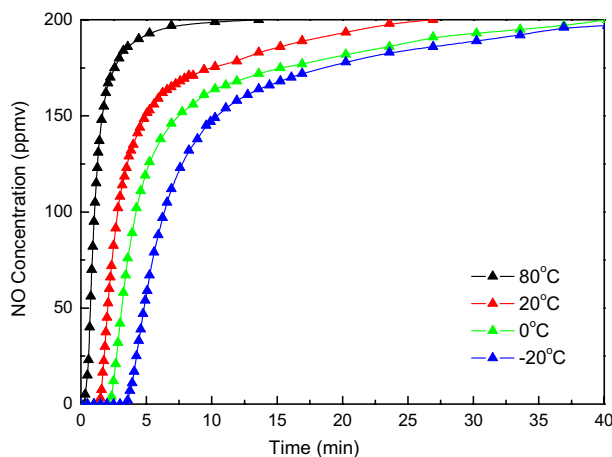


Figure 6. Breakthrough curve of NO adsorption at 80, 20, 0 and -20 °C (NO = 200 ppmv, space velocity = 5000 h⁻¹).

Temperature (°C)	NO adsorption			NO–O ₂ co-adsorption			
	<i>t_b</i> (min)	<i>A_b</i> (mg/g)	<i>A_s</i> (mg/g)	<i>t_b</i> (min)	<i>A_b</i> (mg/g)	<i>A_s</i> (mg/g)	$\eta(\text{NO}_2)$ (%)
80	0.25	0.011	0.066	3.49	0.156	3.765	2.0
20	1.38	0.062	0.213	55.82	2.492	45.333	45.0
0	2.17	0.097	0.332	392.40	17.518	116.349	69.0
-20	3.42	0.153	0.434	1591.75	71.061	169.142	91.5

Table 4. Adsorption characteristics of NO and NO–O₂ over CAC at various temperatures (NO = 200 ppmv, O₂ = 6 vol.%, space velocity = 5000 h⁻¹).

Based on the observation from Fig. 5 and Table 3, it is found that the specific capacity of both NO and SO₂ increases substantially with decreasing temperature. At above room temperature, the specific capacity of NO is less than 1 mg/g, which is insufficient for adsorption removal. At -20 °C, the specific capacity of NO increases to 13.24 mg/g, and the removal of NO_x from flue gas through adsorption becomes possible. At above room temperatures, the breakthrough time of NO is much shorter than that of SO₂. At -20 °C, although the specific capacity of NO is far smaller than that of SO₂, the breakthrough time of NO is close to that of SO₂. This is because the concentration of SO₂ is much higher than NO in the flue gas. Therefore, it is technically feasible to remove SO₂ and NO_x by adsorption at cold temperatures.

The above experiments reveal the phenomenon of simultaneous adsorption of NO and SO₂ in simulated flue gas. To understand the mechanism of NO and SO₂ adsorption at cold temperatures, the adsorption of NO and SO₂ are studied and discussed separately in sections “Adsorption of NO” and “Adsorption of SO₂”.

Adsorption of NO. Figure 6 shows the breakthrough curves of the NO adsorption over CAC at 80, 20, 0 and -20 °C. 6 g of pretreated CAC is loaded in the adsorption tubes and the space velocity is 5000 h⁻¹. The inlet gas has flow rate of 1 L/min, and is composed of NO and N₂, with an concentration of $C_m(\text{NO}) = 200$ ppmv. The concentration of NO at the outlet of adsorption bed is measured and plotted in Fig. 6. The breakthrough time and adsorption capacity of NO adsorption is given in Table 4. The physisorption (Van der Waals adsorption) of NO over activated carbon is enhanced by decreasing the adsorption temperature since physisorption is an exothermic process²¹. Without the presence of oxygen, the specific capacity of NO physisorption is less than 0.5 mg/g even at -20 °C.

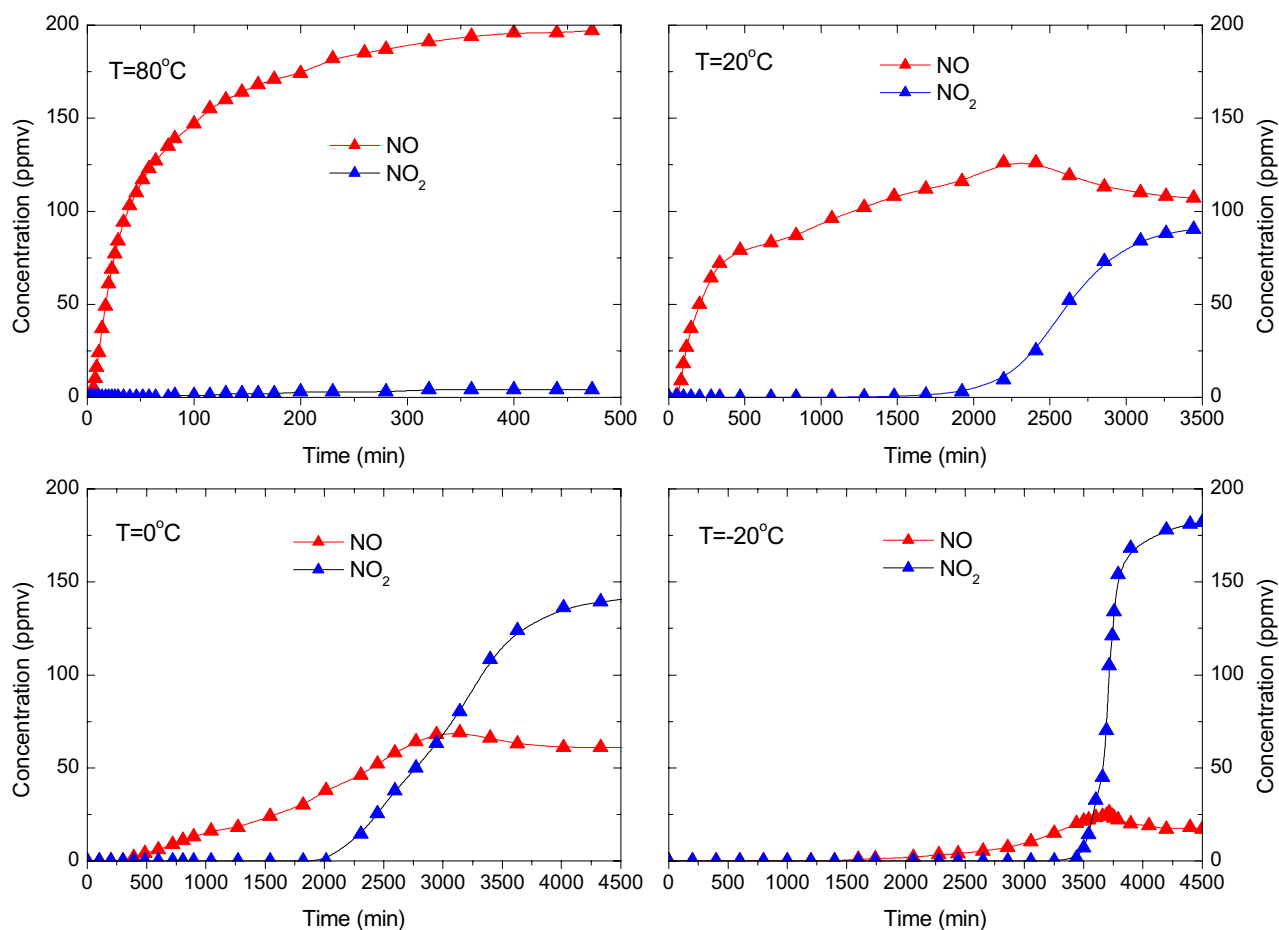


Figure 7. Breakthrough curves of NO (red) and NO₂ (blue) during NO–O₂ co-adsorption at 80, 20, 0 and –20 °C (NO = 200 ppmv, O₂ = 6 vol.%, space velocity = 5000 h⁻¹).

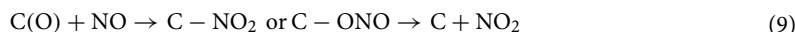
Figure 7 shows the breakthrough curves of the NO–O₂ co-adsorption over CAC at 80, 20, 0 and –20 °C. 6 g of pretreated CAC is loaded in the adsorption tube and the space velocity is 5000 h⁻¹. The inlet gas has flow rate of 1 L/min, and is composed of NO (200 ppmv), O₂ (6 vol.%) and N₂. With the presence of oxygen, NO can be oxidized to NO₂ over activated carbon^{22,23}, a steady NO–NO₂ equilibrium will be formed at the exit of activated carbon bed^{24,25}. Therefore, the concentration of both NO and NO₂ at the outlet of adsorption bed is measured and plotted in Fig. 7. At 80 °C, NO (red) breakthrough the adsorption bed within a few minutes and reaches a steady concentration after about 400 min, and about 2% of NO is oxidized to NO₂. At 20 °C, NO (red) breakthrough the bed after about 56 min, and NO₂ (blue) is detected after about 1600 min. After about 3500 min, both NO and NO₂ reaches a steady concentration and the oxidation rate of NO is about 45%. When adsorption temperature is lowered to 0 °C and –20 °C, the breakthrough time of NO increases to 392 and 1591 min, respectively. Meanwhile, the oxidation rate of NO increases to 69% and 91.5%, respectively. For each test, the sum of NO and NO₂ concentration is 200 ppmv when the steady state is reached.

The adsorption capacity of NO–O₂ co-adsorption at various temperatures is given in Table 4. Both NO and NO₂ has a breakthrough time during NO–O₂ co-adsorption, as shown in Fig. 7. The breakthrough time for NO–O₂ co-adsorption is defined as the breakthrough of NO which always occurs first. The breakthrough adsorption capacity A_b is calculated by Eq. (5) and the saturated adsorption capacity A_s is calculated by Eq. (6), where $C_{out}(t) = C_{out}(NO_x) = C_{out}(NO) + C_{out}(NO_2)$ in the case of NO–O₂ co-adsorption.

As shown in Table 4, the presence of oxygen can significantly increase the breakthrough time and specific capacity of NO. With presence of oxygen, NO can be oxidized to NO₂ which is a much more adsorbable species over activated carbon^{26,27}. The oxidation rate $\eta(NO_2)$ is calculated by the following equation:

$$\eta(NO_2) = \frac{C_{out}(NO_2)}{C_{in}(NO)} \times 100\% \quad (7)$$

where $C_{out}(NO_2)$ is the concentration of NO₂ when it reaches steady state. $C_{in}(NO)$ is the inlet NO concentration. The oxidation rate of NO at 80, 20, 0 and –20 °C is given in Table 4 as well. With the presence of oxygen, the catalytic oxidation of NO is significantly enhanced by at sub-zero temperatures. The mechanism of NO oxidation over activated carbon is complicated, involving both surface reactions and gaseous reactions. The oxidation of gaseous NO by adsorbed oxygen over the activate surface site is believed to be the dominant pathway²⁶.



where $C(\cdot)$ represents the activated carbon with active surface site. Based on reaction (9), the oxidation reaction rate can be calculated by the following equation:

$$\frac{d[NO_2]}{dt} = k(T)[C(O)] \times [NO] \quad (10)$$

Temperature can impact the oxidation reactions in many ways. First of all, the physisorption of oxygen over activated carbon is enhanced and the concentration of $C(O)$ is increased by reducing adsorbing temperature²⁸. Secondly, the rate constant $k(T)$ of NO oxidation increases with decreasing temperature²⁹.

As shown in Table 4, temperature has a significant impact on the breakthrough time and specific capacity of NO–O₂ co-adsorption. When the adsorption temperature decreases from 80 to –20 °C, the breakthrough time increases from 3.5 to 1591 min, and the saturated capacity increases from 3.8 to 169 mg/g. This extraordinary increase of specific capacity is due to the NO₂ adsorption.

Figure 8 shows the breakthrough curves of the NO–O₂ co-adsorption over CAC with various loading space velocity. In Fig. 8a, 0.25 g CAC is loaded and the space velocity is 120,000 h^{–1}; in Fig. 8b, 0.5 g CAC is loaded and the space velocity is 60,000 h^{–1}; in Fig. 8c, 1 g CAC is loaded and the space velocity is 30,000 h^{–1}; in Fig. 8d, 2 g CAC is loaded and the space velocity is 15,000 h^{–1}; in Fig. 8e, 4 g CAC is loaded and the space velocity is 7500 h^{–1}; in Fig. 8f, 6 g CAC is loaded and the space velocity is 5000 h^{–1}. All six experiments are conducted at –20 °C. The inlet gas has flow rate of 1 L/min, and is composed of NO (200 ppmv), O₂ (6 vol.%) and N₂.

The purpose of conducting these six independent experiments is to mimic the experiment of simultaneously motoring NO and NO₂ at six different cross sections of a single adsorption bed which is difficult to achieve in our experimental setup.

The average adsorption capacity and oxidation rate along the axial direction of the CAC bed are given in Fig. 9 and Table 5. As shown in Fig. 9, the NO₂ concentration increases along the bed, indicating that the oxidation rate increases along the axial direction of the adsorption bed. At each cross section of the adsorption bed, a stable NO–NO₂ equilibrium is formed both in the gas phase and the adsorption surface. Therefore the NO–O₂ co-adsorption mechanism involves the adsorption of both NO and NO₂ over activated carbon. Since NO₂ is a much more adsorbable species than NO³⁰, the adsorption capacity increases with the increasing NO₂ concentration along the axial direction of activated carbon bed, as shown in Fig. 9. This is quite different with the adsorption of SO₂ which has a uniform adsorption capacity along the adsorption bed. Due to this distinct characteristics, it should be noted that the adsorption capacity given in Fig. 9 and Table 5 should be defined as average adsorption capacity of a specific CAC bed. The real adsorption capacity at each cross section should be larger than the average value.

Based on the above analysis, it is now quite clear why the breakthrough time and adsorption capacity of NO–O₂ co-adsorption increases dramatically when the adsorption temperature is lowered to below room temperatures. At cold temperatures, the catalytic oxidation of NO is fastened, therefore the breakthrough time and breakthrough adsorption capacity are largely increased. In addition, the adsorption capacity of NO₂ increases significantly at cold temperatures, leading to prominent increase of saturated adsorption capacity.

Adsorption of SO₂. Figure 10 shows the breakthrough curves of the SO₂ adsorption over CAC at 80, 20, 0 and –20 °C. 6 g of pretreated CAC is loaded in the adsorption tube and the space velocity is 5000 h^{–1}. The inlet gas has flow rate of 1 L/min, and is composed of SO₂ (1000 ppmv), O₂ (6 vol.%) and N₂. The concentration of SO₂ at the outlet of adsorption bed is measured and plotted in Fig. 10. Results indicate that the breakthrough time and specific capacity of SO₂ adsorption increases with decreasing temperature. When the temperature decreases from 80 to –20 °C, the breakthrough time and adsorption capacity increase by about 13 and 10 times, respectively. SO₂ adsorption over activated carbon is fast and the breakthrough adsorption capacity is quite close to the saturated adsorption capacity. The breakthrough curve has a sharp slope which is quite different with that of NO adsorption.

The impact of O₂, CO₂ and H₂O on the adsorption of SO₂ at various temperatures are also investigated. As shown in Table 6, the presence of oxygen has a slight improvement of SO₂ adsorption due to the catalytic oxidation over activated carbon. The presence of CO₂ in the opposite has a negative impact on the SO₂ adsorption due to the occupation of active carbon surface. The presence of H₂O and O₂ can enhance the adsorption of SO₂ through H₂SO₄ adsorption⁹.

The impact of space velocity of CAC load on the adsorption of SO₂ is shown in Fig. 11. The breakthrough time is doubled when the CAC load is doubled. This indicates that the adsorption capacity (mg/g CAC) is irrelevant with space velocity and is a constant value at certain temperature and partial pressure of SO₂. This is also quite different with the adsorption capacity of NO (with the presence of O₂) which increases along the adsorption bed as shown in Fig. 9.

The adsorption process of SO₂ and NO with the presence of oxygen over activated carbon is illustrated in Fig. 12. There are three regions during the SO₂ adsorption process (upleft). In the saturated region, an equilibrium of [SO₂(g), SO₂(a)] is established. Where (g) present gaseous phase and (a) represent adsorbed phase. In the adsorption region, SO₂(g) is being adsorbed and converted to SO₂(a). Since the adsorption of SO₂ is fast, the adsorption region is within a narrow region. In the fresh carbon region, both SO₂(g) and SO₂(a) are zero. When the adsorption bed reaches the saturated status (upright), a homogeneous equilibrium of SO₂(g) and SO₂(a) is established cross the entire adsorption bed:

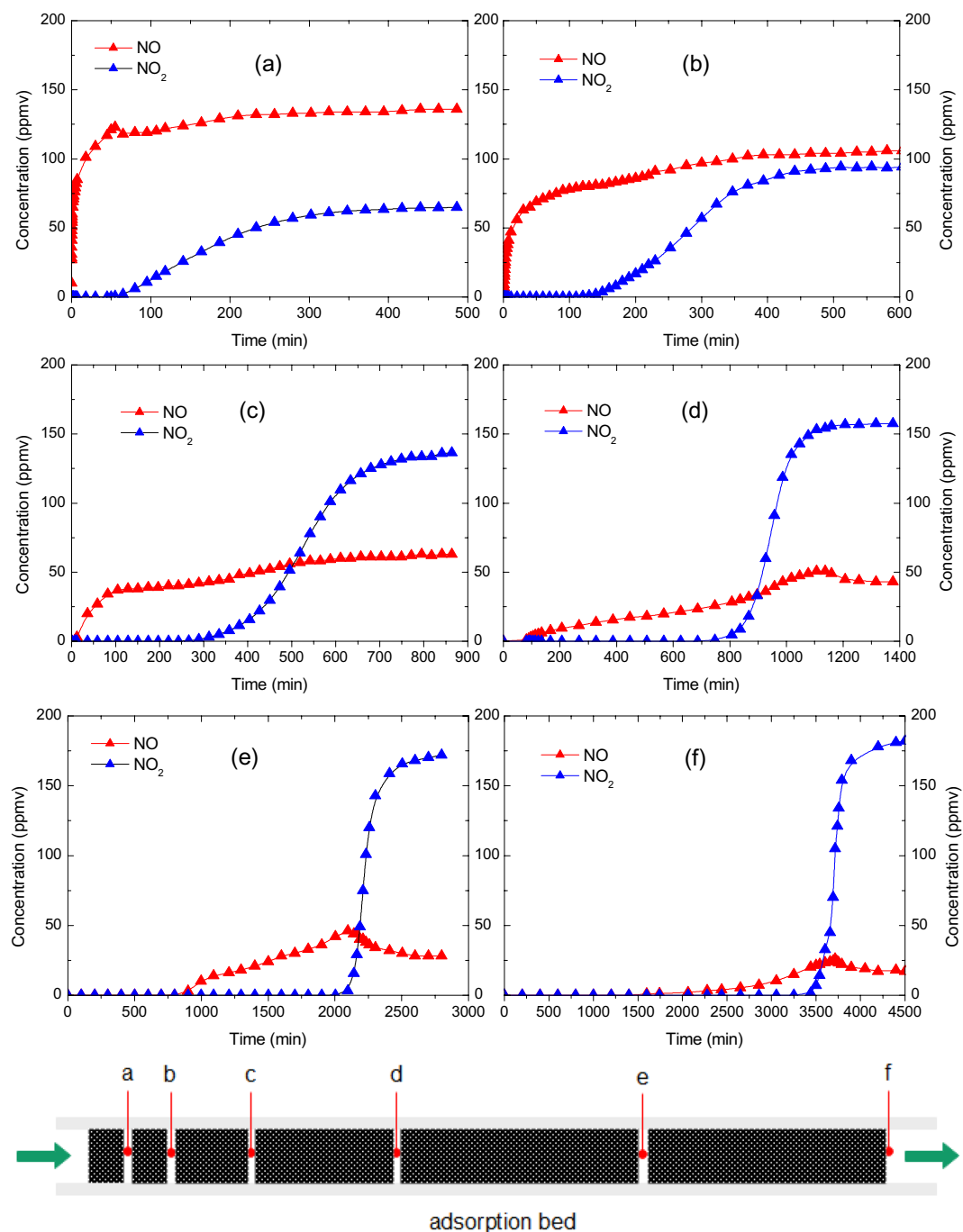


Figure 8. Breakthrough curves of NO (red) and NO₂ (blue) during NO–O₂ co-adsorption at various cross sections of adsorption bed: (a) 120,000 h⁻¹, (b) 60,000 h⁻¹, (c) 30,000 h⁻¹, (d) 15,000 h⁻¹, (e) 7500 h⁻¹ and (f) 5,000 h⁻¹ (NO = 200 ppmv, O₂ = 6 vol.%, T = - 0°C).



For NO + O₂ adsorption (lower left), due to the catalytic oxidation, equilibria of [NO(g), NO(a)] and [NO₂(g), NO₂(a)] co-exist, with increasing NO₂ and decreasing NO along the bed. Since the adsorption of NO is almost neglectable compared with NO₂, the total adsorption capacity increases along the adsorption bed in the saturated region. In the adsorption region, the remaining NO is further oxidized to NO₂ and adsorbed. Since the adsorption rate is limited by oxidation rate, the adsorption of NO + O₂ is much slower than SO₂ and the adsorption region is much wider. When it reaches saturated status, equilibrium of [NO(g), NO(a)] with decreasing partial pressure and equilibrium of [NO₂(g), NO₂(a)] with increasing partial pressure are established along the adsorption bed. At each cross section of the bed, the following equilibria co-exist:

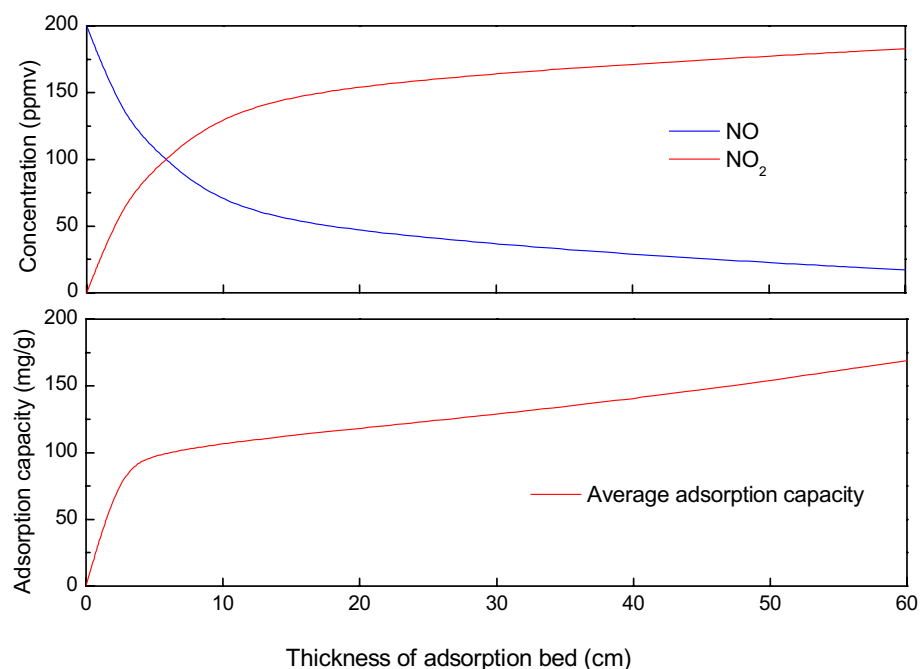


Figure 9. Oxidation and adsorption characteristics of NO–O₂ along activated carbon bed (NO = 200 ppmv, O₂ = 6 vol.%, T = – 20 °C, space velocity = 5000 h⁻¹ when thickness is 60 cm).

Mass of CAC (g)	Space velocity (h ⁻¹)	NO–O ₂ adsorption			
		t _b (min)	A _b (mg/g)	A _s (mg/g)	η(NO ₂) (%)
0.25	120,000	0.01	0.011	88.091	32.0
0.5	60,000	0.44	0.236	98.476	47.0
1	30,000	10.86	2.909	107.356	68.5
2	15,000	88.42	11.841	118.259	78.5
4	7,500	973.18	65.169	138.999	86.0
6	5,000	1591.75	71.061	169.142	91.5

Table 5. Adsorption characteristics of NO–O₂ at various CAC load (NO = 200 ppmv, O₂ = 6 vol.%, T = – 20 °C).

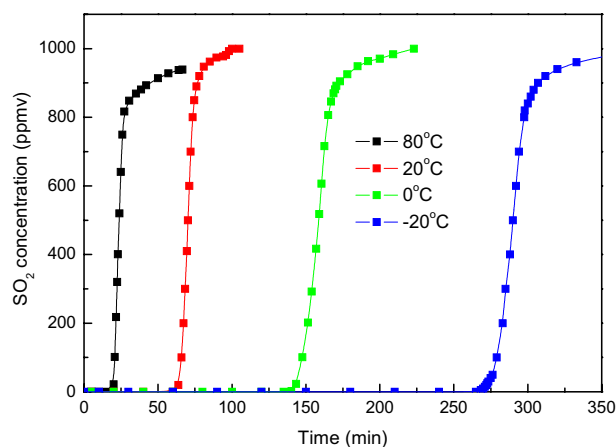


Figure 10. Breakthrough curve of SO₂ adsorption over CAC at various temperatures (SO₂ = 1000 ppmv, O₂ = 6 vol.%, flow rate = 1 L/min, space velocity = 5000 h⁻¹).

Temperature (°C)	SO ₂		SO ₂ -O ₂		SO ₂ -O ₂ -H ₂ O		SO ₂ -CO ₂	
	t _b (min)	A _s (mg/g)	t _b (min)	A _s (mg/g)	t _b (min)	A _s (mg/g)	t _b (min)	A _s (mg/g)
80	19	12.87	20	13.29	28	18.25	18	11.89
20	57	29.88	61	33.97	62	34.32	52	28.69
0	130	67.72	138	76.40	138	73.02	109	58.74
-20	235	123.11	265	140.32	269	140.17	188	108.27

Table 6. Adsorption characteristics of SO₂ over activated carbon (SO₂ = 1000 ppmv, O₂ = 6 vol.%, CO₂ = 12 vol.%, space velocity = 5000 h⁻¹) (H₂O: 10 vol.%, 2.3 vol.% saturated, 0.6% saturated and 0.1 vol.% saturated at 80, 20, 0 and - 20 °C).

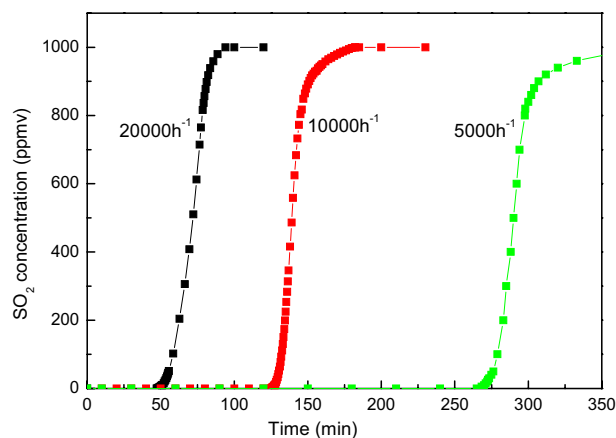


Figure 11. Breakthrough curve of SO₂ adsorption over CAC at various space velocity (SO₂ = 1000 ppmv, O₂ = 6 vol.%, T = - 20 °C, flow rate = 1 L/min).

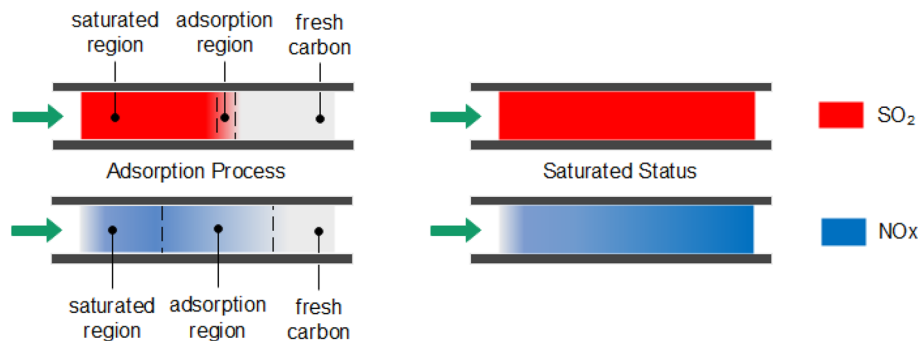


Figure 12. Adsorption process of SO₂ (red) and NO (blue) with presence of oxygen over activated carbon.



Pilot test. The pilot test platform is built in Huaneng Yueyang Power Plant and is accomplished in September 2020. A detail description of the process is given in section “Pilot platform”. A picture of the pilot test

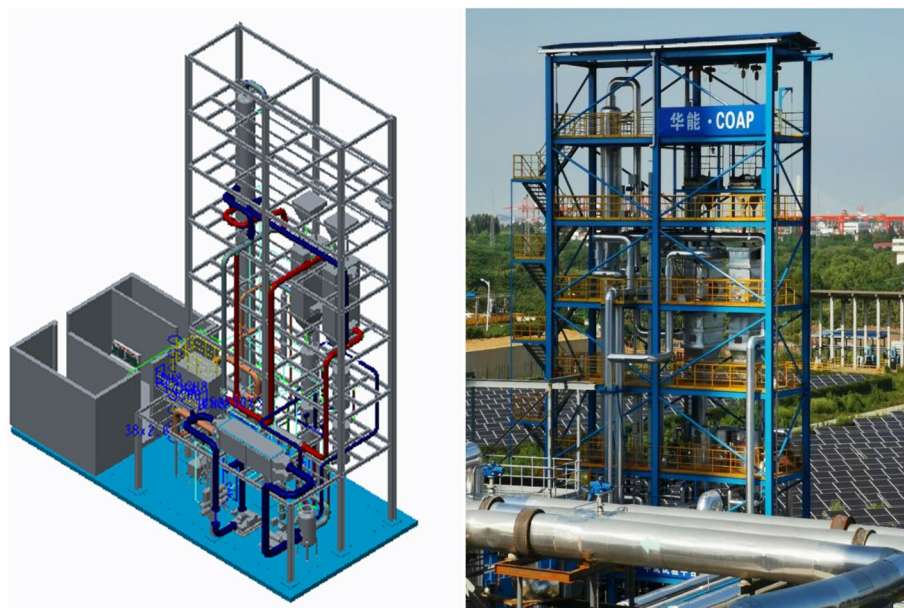


Figure 13. 3D model (left) and a photo (right) of the pilot test platform.

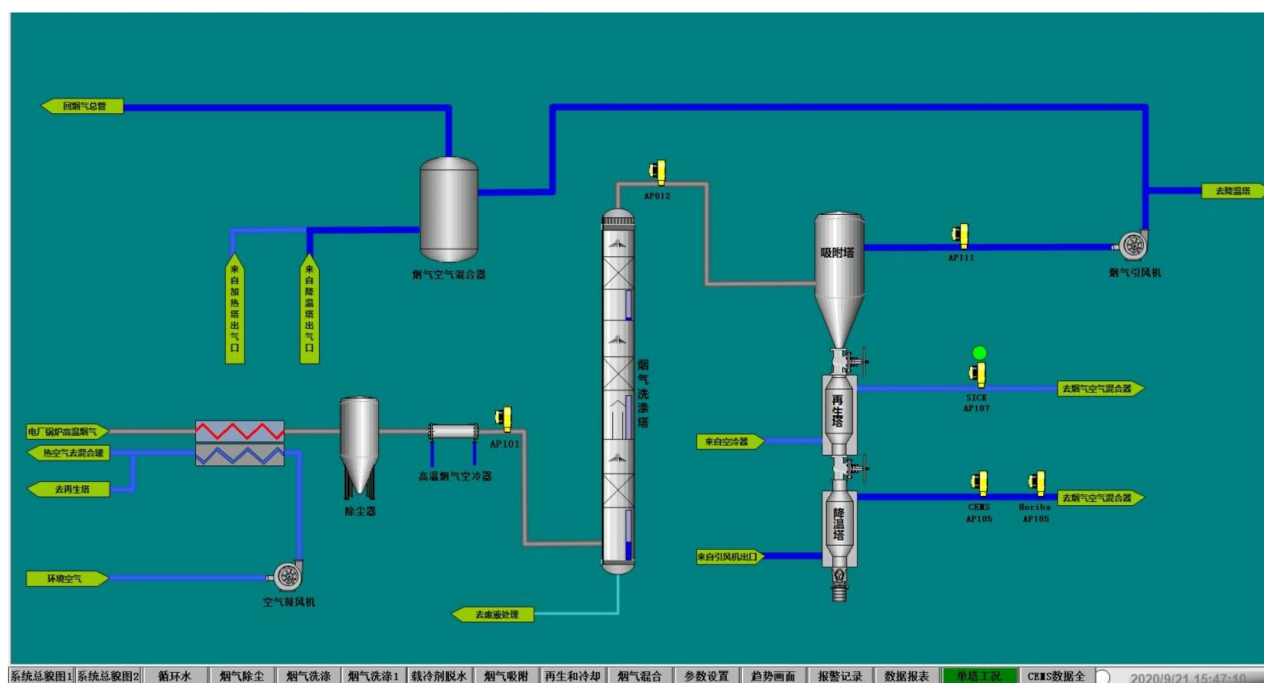


Figure 14. Process diagram of the low-temperature adsorption system.

platform is shown in Fig. 13. A preliminary low-temperature adsorption test is conducted in October. The flue gas flow rate is $3600 \text{ Nm}^3/\text{h}$ and the operating temperature is -15 to -20 °C. Figure 14 is simplified process diagram of the pilot system. Figure 15 shows the inlet and outlet flue gas composition monitored by online CEMS system. Figures 16 and 17 shows some of the operating data of a successive 72 h test. The inlet flue gas has an SO_2 concentration of around 500–1000 ppmv and NO_x concentration of around 70–100 ppmv. The concentrations of both SO_2 and NO_x are reduced to below 1 ppmv when leaving the adsorber. More tests are undergoing and will be shared as soon as the data are unclassified. In addition, the performance and energy penalty are evaluated by conducting Aspen Plus modeling, and the energy penalty is about 2–3% of the total net power generation depending on the ambient temperatures. The detail data of the pilot test and the modeling work will be presented and discussed shortly.

烟气分析系统数据 FG Analysis System			
烟气入口分析仪 FG Inlet		烟气出口分析仪 FG Outlet	
SO ₂	1940.57mg/m ³	SO ₂	0.88mg/m ³
NO	156.20mg/m ³	NO	0.22mg/m ³
NO _x	239.51mg/m ³	NO _x	0.34mg/m ³
PM	12.50mg/m ³	PM	2.10mg/m ³
O ₂	7.92%	O ₂	8.97%

Figure 15. Inlet and outlet flue gas composition monitored by online CEMS system.

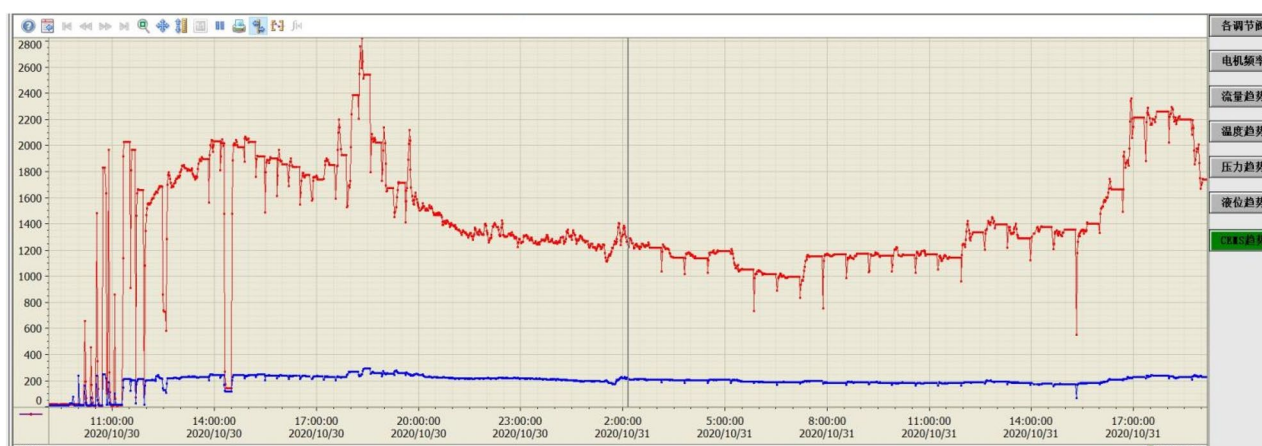


Figure 16. SO₂ (red) and NO_x (blue) concentration of inlet flue gas during 72-h operation.

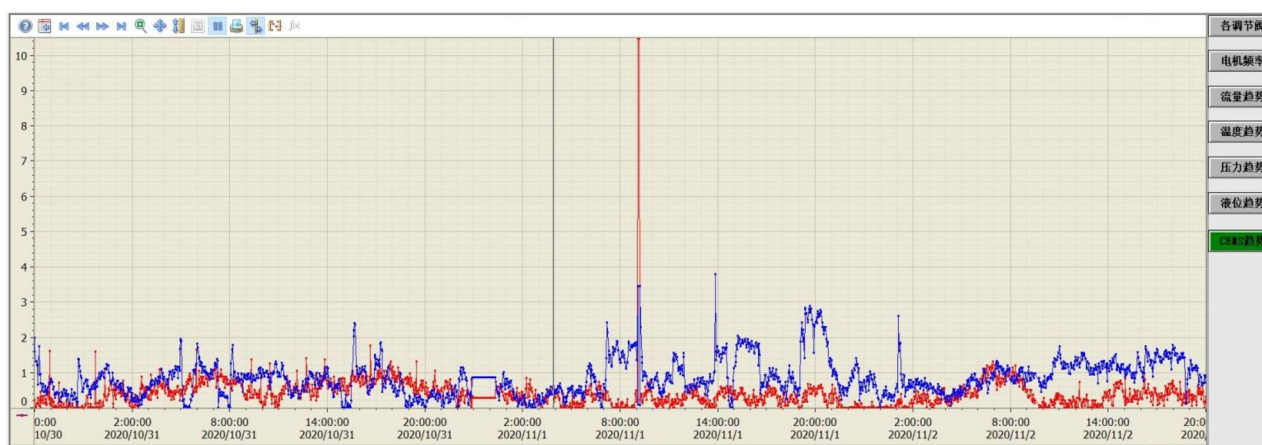


Figure 17. SO₂ (red) and NO_x (blue) concentration of outlet flue gas during 72-h operation.

Conclusion

In this study, the oxidation and adsorption characteristics of NO over activated carbon at cold temperatures is investigated. With the presence of oxygen, both the oxidation rate and adsorption of NO over activated carbon is enhanced significantly at cold temperatures. The breakthrough time of NO increases from 3.45 to 1591.75 min when the adsorption temperature decreases from 80 to -20°C . At each cross sections along the adsorption bed,

NO and NO₂ equilibrium is established with decreasing NO and increasing NO₂ along the bed, which leads to an increasing adsorption capacity along the bed. The adsorption of SO₂ also increases significantly at cold temperatures. The adsorption capacity increases from 12.87 to 123.11 mg/g when the temperature decreases from 80 to -20 °C. A novel low-temperature adsorption process is developed to simultaneously remove SO₂ and NO_x from flue gas. A pilot scale test platform is built and the low-temperature adsorption process is tested. Near-zero emission of both SO₂ and NO_x is achieved during a 72 h performance validation test.

Received: 16 November 2020; Accepted: 26 April 2021

Published online: 26 May 2021

References

1. Srivastava, R. & Jozewicz, W. Flue gas desulfurization: the state of the art. *J. Air Waste Manag. Assoc.* **2002**(51), 1676–1688 (1995).
2. Wang, E., Lei, S., Zhong, L. & Zhang, S. Review of advanced technology of flue gas desulfurization. *Adv. Mater. Res.* **852**, 86–91 (2014).
3. Flagiello, D. Seawater desulfurization of simulated flue gas in spray and packed columns: an experimental and modelling comparison. *Chem. Eng. Trans.* <https://doi.org/10.3303/CET1869134> (2018).
4. Flagiello, D. *et al.* Seawater desulfurization scrubbing in spray and packed columns for a 4.35 MW marine diesel engine. *Chem. Eng. Res. Des.* **148**, 56–67 (2019).
5. Guo, L., Shu, Y. & Gao, J. Present and future development of flue gas control technology of DeNO_x in the world. *Energy Proc.* **17**, 397–403 (2012).
6. Tsuji, K. & Shiraishi, I. Combined desulfurization, denitrification and reduction of air toxics using activated coke: 1. Activity of activated coke. *Fuel* **76**(6), 549–553 (1997).
7. Tsuji, K. & Shiraishi, I. Combined desulfurization, denitrification and reduction of air toxics using activated coke: 2. Process applications and performance of activated coke. *Fuel* **76**(6), 555–560 (1997).
8. Olson, D., Tsuji, K. & Shiraishi, I. The reduction of gas phase air toxics from combustion and incineration sources using the MET-Mitsui-BF activated coke process. *Fuel Process. Technol.* **65**(66), 393–405 (2000).
9. Sun, F., Gao, J., Zhu, Y. & Qin, Y. Mechanism of SO₂ adsorption and desorption on commercial activated coke. *Korean J. Chem. Eng.* **28**, 2218–2225 (2011).
10. Wang, X., Piao, G., Xie, H. & Zhao, X. Selective catalytic reduction of NO_x by activated carbon. *J. Southeast Univ. (Nat. Sci. Edn.)* **41**, 145–149 (2011).
11. Zhu, T., Xu, W., Guo, Y. & Li, Y. Pollutants emission and control for sintering flue gas. In *Ironmaking and Steelmaking Processes* (ed. Cavaliere, P.) (Springer, Cham, 2016).
12. Jiang, J. C., Jiang, X. & Yang, Z. S. Flue gas desulfurization and denitrification by activated coke: a mini-review. *Rec. Patents Chem. Eng.* **6**(3), 143–151 (2013).
13. Xu, Z. *et al.* An efficient and sulfur resistant K-modified activated carbon for SCR denitrification compared with acid- and Cu-modified activated carbon. *Chem. Eng. J.* **395**, 125047 (2020).
14. Zuo, Y., Yi, H. & Tang, X. Metal-modified active coke for simultaneous removal of SO₂ and NO_x from sintering flue gas. *Energy Fuels* **29**, 377–383 (2015).
15. Mochida, I. *et al.* Removal of SO₂ and NO_x over activated carbon fibers. *Carbon* **38**, 227–239 (2013).
16. Chengxue, W. & Zhenheng, D. Studies on HZSM-5 zeolite catalysts for desulfurization and denitrification. In *2011 International Conference on Consumer Electronics, Communications and Networks (CECNet)* 4429–4432. IEEE (2011).
17. Penkova, A. *et al.* FTIR spectroscopic study of low temperature NO adsorption and NO+O₂ coadsorption on H-ZSM-5. *Langmuir ACS J. Surf. Colloids* **20**, 5425–5431 (2004).
18. Tseng, H.; Haslbeck, J.; Neal, L., Evaluation of the NOXSO combined NO_xSO flue gas treatment process: process chemistry, reaction kinetics, sorbent performance, process design and cost analysis. Final report. [Alumina substrate impregnated with sodium carbonate]. **2020**.
19. Liu, D., Chen, S., Fei, X., Huang, C. & Zhang, Y. Regenerable CuO-based adsorbents for low temperature desulfurization application. *Ind. Eng. Chem. Res.* **54**, 3556–3562 (2015).
20. Mochida, I., Ogaki, M., Fujitsu, H., Komatsubara, Y. & Ida, S. Catalytic activity of coke activated with sulphuric acid for the reduction of nitric oxide. *Fuel* **62**, 867–868 (1983).
21. Condon, J. B. An overview of physisorption. *Surf. Area Porosity Determ. Physisorp. Meas. Theory* **1**, 1–27 (2006).
22. Fang, Z., Yu, X. & Tu, S.-T. Catalytic oxidation of NO on activated carbons. *Energy Proc.* **158**, 2366–2371 (2019).
23. Dastgheib, S. A., Salih, H., Ilangovan, T. & Mock, J. NO oxidation by activated carbon catalysts: impact of carbon characteristics, pressure, and the presence of Water. *ACS Omega* **5**(33), 21172–21180 (2020).
24. Guo, Z.-C., Xie, Y., Hong, I. & Kim, J. Catalytic oxidation of NO to NO₂ on activated carbon. *Energy Convers. Manage.* **42**, 2005–2018 (2001).
25. Sousa, J., Pereira, M. & Figueiredo, J. Catalytic oxidation of NO to NO₂ on N-doped activated carbons. *Catal. Today* **176**, 383–387 (2011).
26. Xu, X. *et al.* Method for the control of NO_x emissions in long-range space travel. *Energy Fuels Am. Chem. Soc. J.* **17**, 1303–1310 (2003).
27. Kong, Y. & Cha, C. NO_x adsorption on char in presence of oxygen and moisture. *Carbon* **34**, 1027–1033 (1996).
28. Park, D., Ju, Y., Kim, J. H., Ahn, H. & Lee, C. H. Equilibrium and kinetics of nitrous oxide, oxygen and nitrogen adsorption on activated carbon and carbon molecular sieve. *Sep. Purif. Technol.* **223**, 63–80 (2019).
29. Tsukahara, H., Ishida, T. & Mayumi, M. Gas-phase oxidation of nitric oxide: chemical kinetics and rate constant. *Nitric Oxide Biol. Chem.* **3**, 191–198 (1999).
30. Sager, U. *et al.* Differences between the adsorption of NO₂ and NO on modified activated carbon. *Gefahrstoffe Reinhalt. Luft* **74**, 181–184 (2014).

Acknowledgements

This study was supported by the China Huaneng Group (Grant Nos. TY-19-HJK01 and TY-19-HJK05).

Author contributions

S.W. discovered the phenomenon and organized this study; S.X., S.G., P.X., M.J. and B.H. contributed significantly on the process design and experiment design. H.Z. L.L., H.N., J.W. and D.G. contributed significantly on the pilot platform design and pilot test. S.W. wrote the manuscript. All authors discussed and commented on the manuscript.

Competing interests

The authors declare no competing interests.

Additional information

Correspondence and requests for materials should be addressed to S.W.

Reprints and permissions information is available at www.nature.com/reprints.

Publisher's note Springer Nature remains neutral with regard to jurisdictional claims in published maps and institutional affiliations.



Open Access This article is licensed under a Creative Commons Attribution 4.0 International License, which permits use, sharing, adaptation, distribution and reproduction in any medium or format, as long as you give appropriate credit to the original author(s) and the source, provide a link to the Creative Commons licence, and indicate if changes were made. The images or other third party material in this article are included in the article's Creative Commons licence, unless indicated otherwise in a credit line to the material. If material is not included in the article's Creative Commons licence and your intended use is not permitted by statutory regulation or exceeds the permitted use, you will need to obtain permission directly from the copyright holder. To view a copy of this licence, visit <http://creativecommons.org/licenses/by/4.0/>.

© The Author(s) 2021